

$$v_{s\beta} = R_s i_{s\beta} + \frac{d\psi_{s\beta}}{dt} \quad (2)$$

$$T_e = p (i_{s\alpha} i_{s\beta} - i_{s\beta} i_{s\alpha}) \quad (3)$$

$$\psi_{s\alpha} = \int (v_{s\alpha} - R_s i_{s\alpha}) dt \quad (4)$$

$$\psi_{s\beta} = \int (v_{s\beta} - R_s i_{s\beta}) dt \quad (5)$$

$$|\vec{\psi}_s| = \sqrt{(\psi_{s\alpha}^2 + \psi_{s\beta}^2)} \quad (6)$$

Herein, R_s is stator phase resistance, p is the number of pole couple, $i_{s\alpha}$, $i_{s\beta}$, $\psi_{s\alpha}$, $\psi_{s\beta}$, $V_{s\alpha}$, $V_{s\beta}$ are current, flux and voltage values on the axis of α - β , T_e is momentum. Amplitude of the vector of the torque and the stator flux calculated with the help of the above equations. The reference value of the stator flux magnitude is compared with the actual flux magnitude. The error obtained is given to a two-level hysteresis comparator. If the error is positive, it implies that the flux magnitude has to be increased and this is denoted as $d\psi=1$. If the error is negative, it implies that the flux magnitude has to be decreased and this is denoted as $d\psi=0$. The flux comparator conditions are given as

$$d\psi = 1 \quad \text{for} \quad |\psi_{ref} - |\psi_s|| \geq |\Delta\psi_s / 2| \quad (7)$$

$$d\psi = 0 \quad \text{for} \quad |\psi_{ref} - |\psi_s|| < |\Delta\psi_s / 2| \quad (8)$$

The rotor reference speed is compared with the feedback speed and by a suitable PI controller this error is converted into reference torque. The reference torque is compared with the real torque and the error obtained is fed to a three-level hysteresis comparator. If the error is positive, it implies that the torque has to be increased and this is denoted by $dt_e=1$. If the error is negative, it implies the torque has to be reduced and this is denoted by $dt_e=-1$. If the error is zero, it implies the torque needs to be constant and this is denoted by $dt_e=0$. The torque comparator conditions are given as

$$dt_e = 1 \quad \text{for} \quad |t_{ref} - |t_e|| \geq |\Delta t_e / 2| \quad (9)$$

$$dt_e = -1 \quad \text{for} \quad |t_{ref} - |t_e|| < |\Delta t_e / 2| \quad (10)$$

$$dt_e = 0 \quad \text{for} \quad |-\Delta t_e / 2| \leq |t_{ref} - |t_e|| \leq |\Delta t_e / 2| \quad (11)$$

To accomplish optimum switching process, one of the 8 different voltage vectors consisting of 8 different switching is selected as seen in Figure 2. V_i (S_a, S_b, S_c) ($i=0,1,2\dots7$) Besides 6 switching levels, there are $V_0(0,0,0)$ and $V_7(1,1,1)$ levels not producing a voltage at the output when they are applied [4].

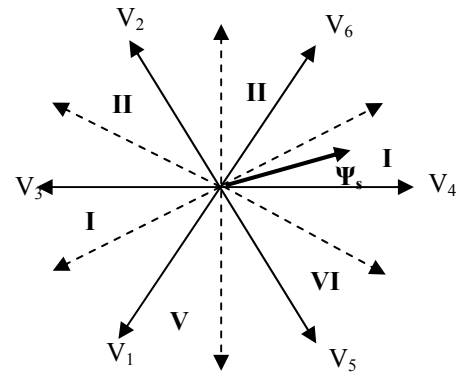


Figure 2. Voltage Space Vector and Sector Representation

Assuming the stator flux linkage space vector to be in sector I and is rotating in counter clockwise direction, the resultant effect of generating different voltage vectors at this instant is given in the Figure 3.

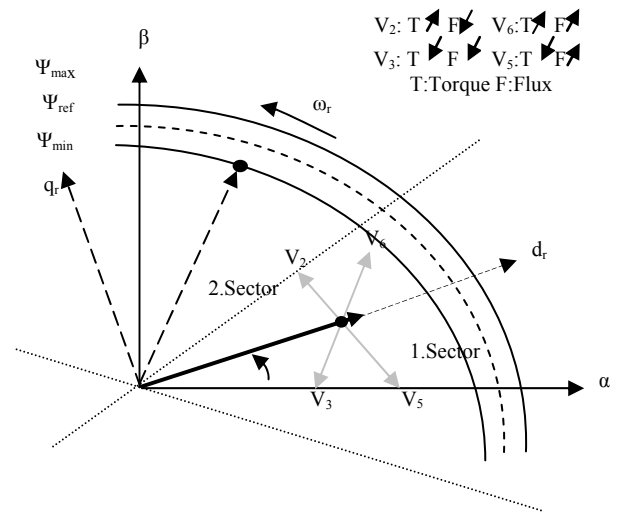


Figure 3. Voltage Space Vector for Flux and Torque Variation

Table 1, which is seen below, shows switching logics when the motor is desired to counter clockwise.

TABLE I
OPTIMAL SWITCHING LOGICS FOR ROTATING COUNTER
CLOCKWISE

		$\theta(1)$	$\theta(2)$	$\theta(3)$	$\theta(4)$	$\theta(5)$	$\theta(6)$
$d\psi = 0$	$dt_e = 1$	V_5	V_1	V_3	V_2	V_6	V_4
	$dt_e = 0$	V_7	V_0	V_7	V_0	V_7	V_0
	$dt_e = -1$	V_6	V_4	V_5	V_1	V_3	V_2
$d\psi = 1$	$dt_e = 1$	V_1	V_3	V_2	V_6	V_4	V_5
	$dt_e = 0$	V_0	V_7	V_0	V_7	V_0	V_7
	$dt_e = -1$	V_2	V_6	V_4	V_5	V_1	V_3

III. FLUX REGION MODIFICATION STRATEGY

In the conventional DTC, although flux is expected to increase in the harmonic during the sector change, it could decrease below the limits of a hysteresis band. Particularly in low speed, the stator flux amplitude moves beyond the flux band interval in every sector change. In order to solve this problem, we propose a method where an angle for the stator flux sector is chosen prior to the sector change. In this method, the flux sector is rotated and the active voltage vector of the previous sector is applied for a while even though the voltage space vector is in a new sector. Therefore, the required stator flux amplitude could be achieved. In Figure 4, we present the new sector formation after rotating first and second sector for a 30 degree[16]. In the conventional DTC, the selection of the voltage vectors depends on only two outputs of the hysteresis control ($d\psi_s$ and dt_e) and the angle of the stator flux space vector (Position of θ_s).

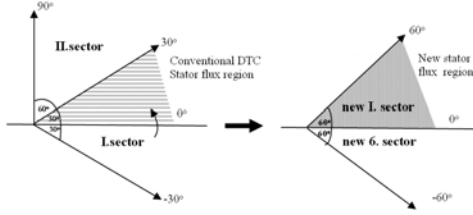


Figure 4. The stator flux regions in the conventional and rotated DTC.

In the method, the relationship between the d axis of the voltage vector applied with outputs of hysteresis control, v_d and its tangent q axis component, v_q is defined. According to this relationship, if $v_d > 0$, the stator flux amplitude will increase and at the same time if $v_q > 0$, the torque will rapidly increase as well. Similar to Figure 3, let the stator flux space vector be initially at A0 and moving counter-clockwise. Then, the flux amplitude is at the lower limit of the hysteresis band. In order to increase the flux amplitude, V2 vector should be selected. When V2 is applied, the position of the stator flux will move to A1. However, the reference value for the flux amplitude has not been achieved yet and there is no other voltage vector that could be applied for achieving that value. This is due to the fact that the V_d component of applied voltage vector at the flux is too small. Since the V_q component is large at the same time, the torque rapidly increases. In the conventional DTC, the output of the torque hysteresis control with same condition provides $dt=0$. As shown in Table 1, the controller selects zero voltage vector and as a result, the flux amplitude drops to the lower values. Creating new flux regions could prevent the decrease in flux at the lower speed[17]. The flux, initially at A1, does not decrease and the flux space vector will move from A1 to A2 as seen in Figure 3. Thus, the decrease in flux is prevented. Table 2 presents new switching table produced by the rotated flux regions.

TABLE 2
MODIFIED SWITCHING LOGICS FOR ROTATING COUNTER
CLOCKWISE

		$\theta(1)$	$\theta(2)$	$\theta(3)$	$\theta(4)$	$\theta(5)$	$\theta(6)$
$d\psi_s=0$	$dt_e=1$	V ₆	V ₂	V ₃	V ₁	V ₅	V ₄
	$dt_e=0$	V ₇	V ₀	V ₇	V ₀	V ₇	V ₀
	$dt_e=-1$	V ₄	V ₆	V ₂	V ₃	V ₁	V ₅
$d\psi_s=1$	$dt_e=1$	V ₃	V ₁	V ₅	V ₄	V ₆	V ₂
	$dt_e=0$	V ₀	V ₇	V ₀	V ₇	V ₀	V ₇
	$dt_e=-1$	V ₁	V ₅	V ₄	V ₆	V ₂	V ₃

IV. MODEL REFERENCE ADAPTIVE SYSTEM (MRAS)

The MRAS technique is used in sensorless IM drivers, at the first time, by Schauder[14]. Figure 5 since this, it has been a topic of many applications [1]. In a MRAS system, some state variables, x_d, x_q (e.g. rotor flux-linkage components, ψ_{ra}, ψ_{rb} or back e.m.f. components, e_d, e_q , etc.) of the induction machine (which are obtained by using measured quantities, e.g. stator voltages and currents) are estimated in a reference model and are then compared with state variables \hat{x}_d, \hat{x}_q estimated by using an adaptive model. The difference between these state variables is then used in an adaptation mechanism, which outputs the estimated value of the rotor speed ($\hat{\omega}_r$) and adjusts the adaptive model until satisfactory performance is obtained. Such a scheme is shown in Fig. 5 where the actual implementation, and here the components of the space vectors are shown. The adaptation mechanism in the Figure 5 is a PI controller[15].

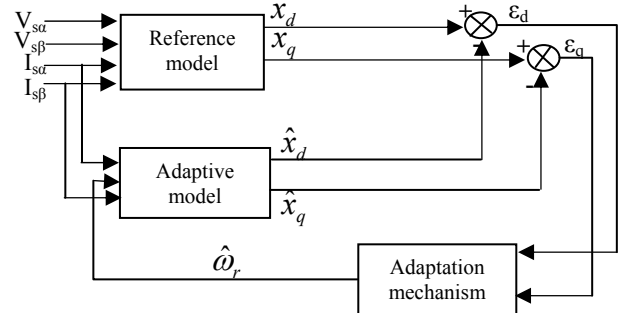


Figure 5. MRAS-based basic speed estimator scheme

A. Rotor Speed Estimator

The rotor speed can be estimated by using two types of estimators (a reference-model-based estimator and an adaptive-model-based one). They independently determine the rotor flux-linkage components in the stator reference frame (ψ_{ra}, ψ_{rb}), and the difference between these flux-linkage estimates are used to drive the speed of the adaptive model. The rotor flux linkages in the stationary reference frame can be obtained by using the stator voltage and current equations of the induction machine in the stationary reference frame. These equations are shown below:

Reference Model:

$$\psi_{r\alpha} = \frac{L_r}{L_m} \left[\int (v_{s\alpha} - R_s i_{s\alpha}) dt - L_s' i_{s\alpha} \right] \quad (16)$$

$$\psi_{r\beta} = \frac{L_r}{L_m} \left[\int (v_{s\beta} - R_s i_{s\beta}) dt - L_s' i_{s\beta} \right] \quad (17)$$

Adaptive Model:

$$\hat{\psi}_{r\alpha} = \frac{1}{T_r} \int (L_m i_{s\alpha} - \hat{\psi}_{r\alpha} - \omega_r T_r \hat{\psi}_{r\beta}) dt \quad (18)$$

$$\hat{\psi}_{r\beta} = \frac{1}{T_r} \int (L_m i_{s\beta} - \hat{\psi}_{r\beta} - \omega_r T_r \hat{\psi}_{r\alpha}) dt \quad (19)$$

Herein, T_r is rotor time constant, L_s is stator circuit leakage inductance, L_r is rotor circuit reduced leakage inductance, L_m is magnetization inductance. The reference and adaptive models are used to estimate the rotor flux – linkages and the angular difference of the outputs of the two estimators $\varepsilon_\omega = \text{Im}(\psi_r \hat{\psi}_r^*) = \psi_{r\beta} \hat{\psi}_{r\alpha} - \psi_{r\alpha} \hat{\psi}_{r\beta}$ is used as the speed tuning signal. This tuning signal is the input to a linear controller (PI controller) which outputs the estimated rotor speed as shown in Figure 6.

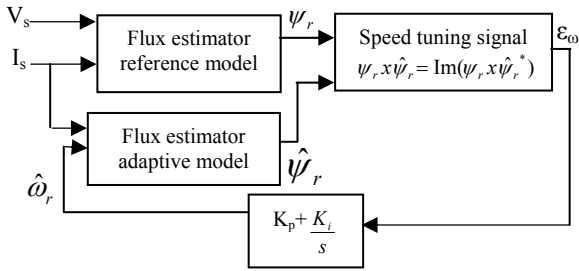


Figure 6. MRAS-based rotor speed observer flux linkages for the speed tuning signal

. When the rotor speed to be estimated ($\hat{\omega}_r$) is changed in the adjustable model in such a way that the difference between

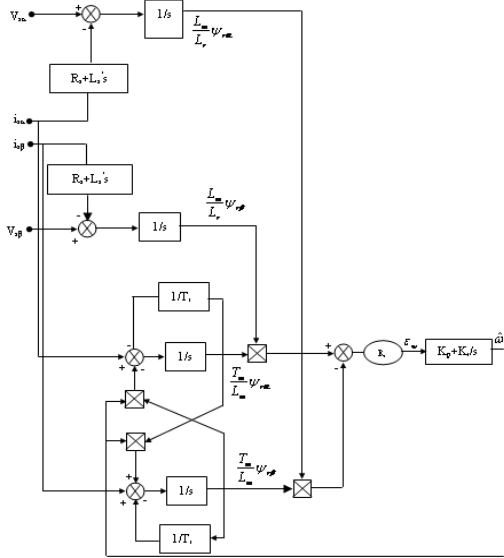


Figure 7. Complete schema of MRAS speed observer using rotor flux linkages

the output of the reference model and the output of the adjustable model becomes zero, then the estimated rotor speed is equal to the actual rotor speed (ω_r). The error signal actuates the rotor-speed identification algorithm, which makes this error converge to zero. Estimated speed can be expressed as

$$\hat{\omega}_r = K_p \varepsilon_\omega + K_i \int \varepsilon_\omega dt \quad (20)$$

Arbitrary K_p and K_i cannot be used to obtain satisfactory performance in this equation. The complete scheme of the flux based MRAS rotor speed observer is shown in Fig.7

In the next sections, we present the simulation and experimental results of the conventional DTC without a sensor and the new method without a sensor and compare their performance.

V. SIMULATION RESULTS

We simulate the conventional DTC and the DTC without a sensor where the flux regions are rotated and compare the results. Figures 8-13 present the transient and steady-state results. Speed reduction is acquired with MRAS and it is observed to be within the reference speed values. In the steady-state, high amplitude ripple disappears. The number of oscillations in current and voltage waves is decreased. Comparing the conventional DTC and DTC using the rotated flux regions without a sensor, the new method provides significant reduction in the flux and torque.

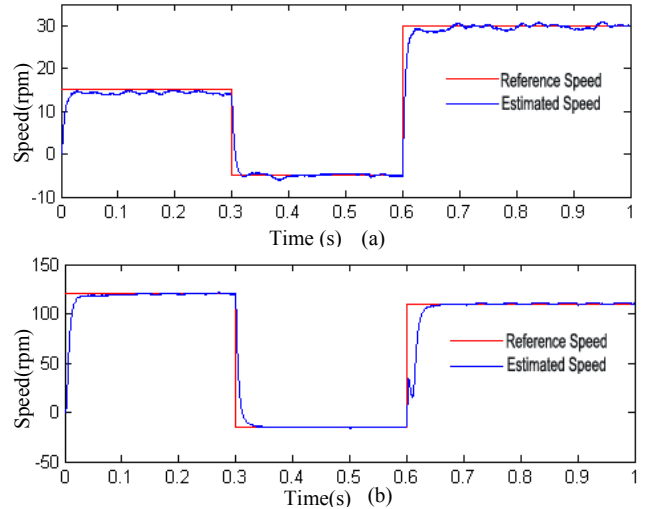
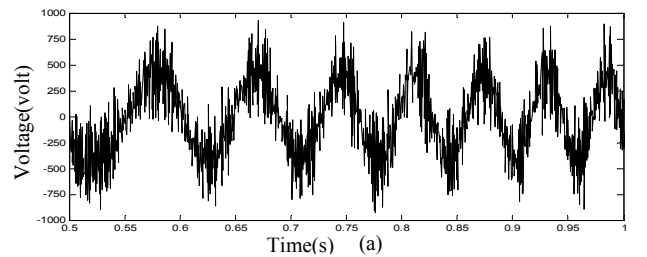


Figure 8. Estimated rotor speed (a)15 rpm, -5 rpm, 30 rpm (b)120 rpm, -15 rpm, 110 rpm



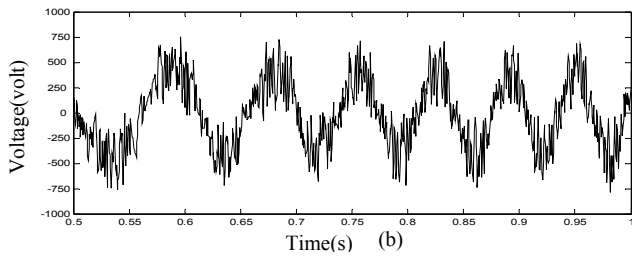


Figure 9. Stator phase voltage V_{ab} (a)Conventional(b)Proposed DTC

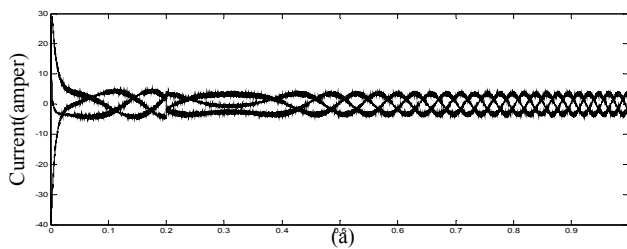
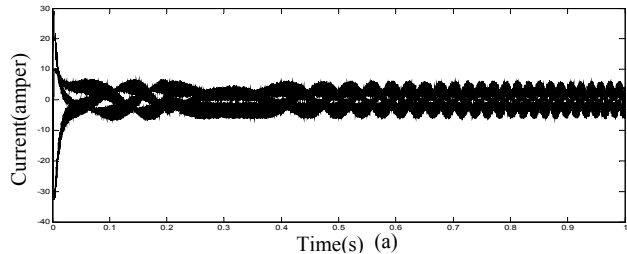


Figure 10. Stator phase currents I_{abc} (a)Conventional(b)Proposed DTC

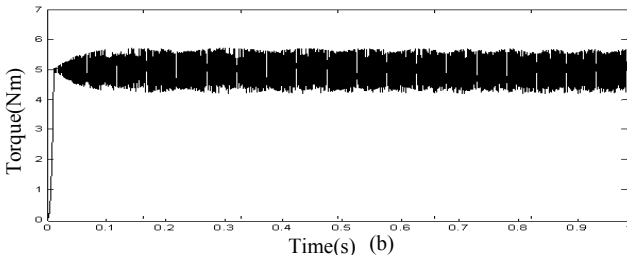
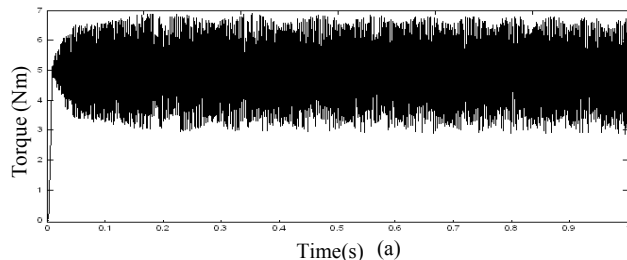


Figure 11. Electromagnetic torque (a)Conventional(b)Proposed DTC

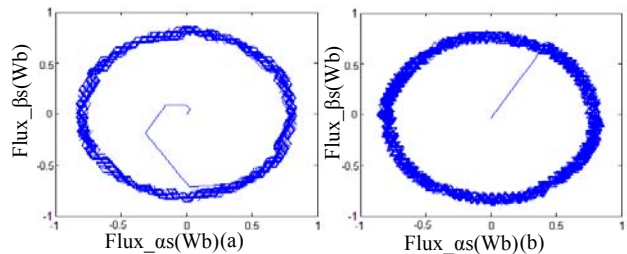


Figure 12. Stator flux locus (a)Conventional(b)Proposed DTC

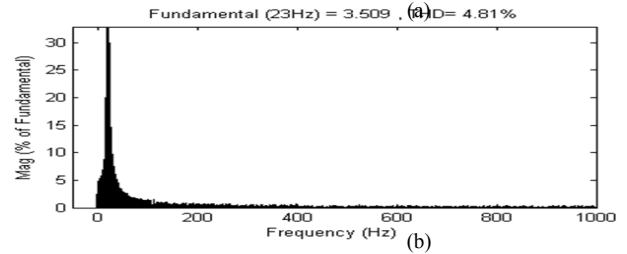
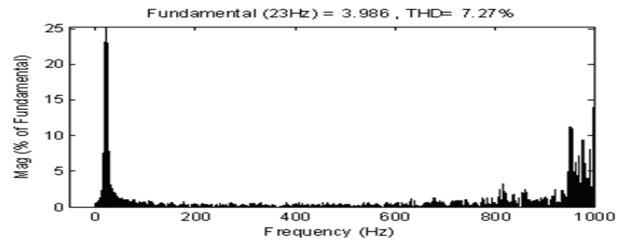


Figure 13. Spectrum of stator current phase A (a)Conventional(b)Proposed DTC

VI. EXPERIMENTAL SETUP

Figure 14 shows the block scheme of the experimental setup. In the experimental setup, each unit is created separately. Then, they are connected to each other. The experimental setup consists of AC-DC engine unit, PC-SCSI communication port, DC-Link capacitor unit, IPM inverter unit, current and voltage circuit unit, reference current and voltage circuit unit, feedback circuit unit and optic isolation unit.

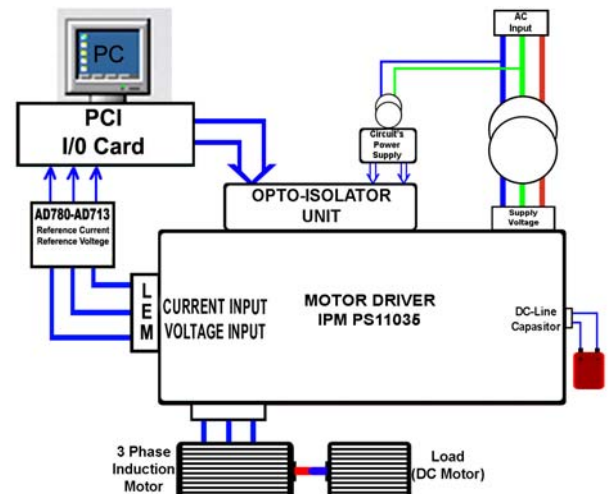


Figure 14. The block schematic of the experimental setup

In the algorithm, necessary voltage and current information from the sensors are obtained using the PCI I/O card. PCI card has 16 analog and digital input channels and 16 digital output channels. Out of all analog input channels, three are used for determining the current and voltage; seven are used for the digital output channel inverter and the control of the inverter signal. Extra information about AC motor and Load motor could be found in Appendix-A. Figure 15 presents the realization of the experimental setup.



Figure 15. Realization of the experimental setup

A. Experimental Results

Next figures 16-19 present the transient and steady-state analyses of experimental results.

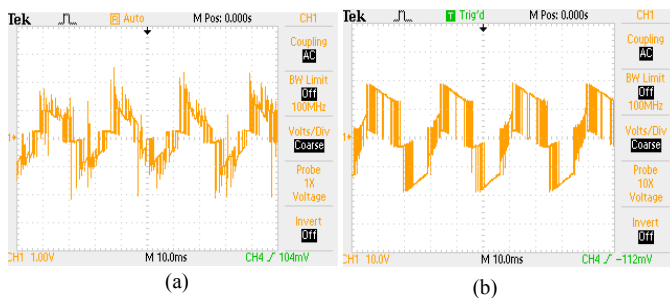


Figure 16. Stator phase voltage V_{ab} (a)Conventional (b)Proposed DTC

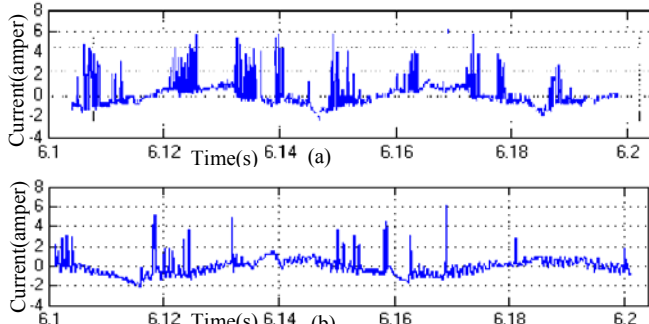


Figure 17. Stator phase currents I_{abc} (a)Conventional (b)Proposed DTC

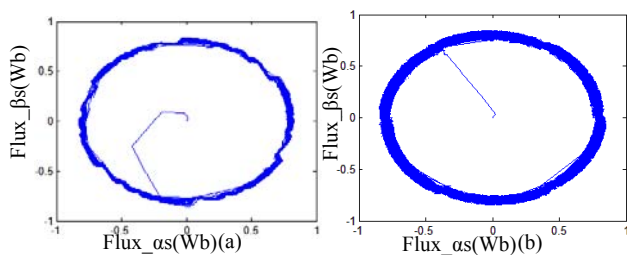


Figure 18. Stator flux locus (a)Conventional (b)Proposed DTC

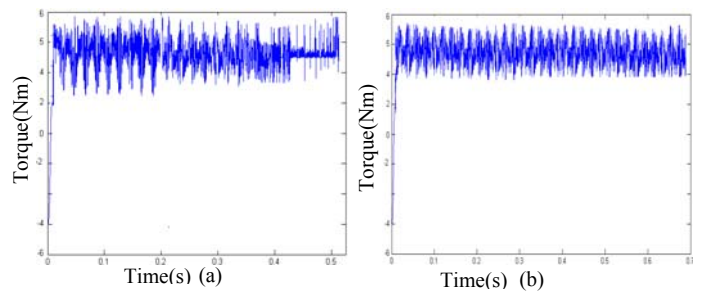


Figure 19. Electromagnetic torque (a)Conventional(b)Proposed DTC

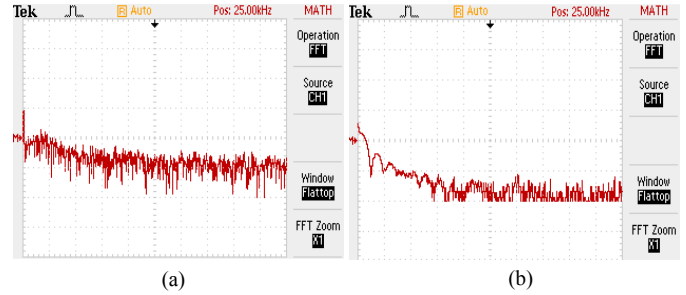


Figure 19. EMI noise level (a)Conventional (b)Proposed DTC

VII. RESULTS

In this study, we eliminate the use of the external sensor. We explored the flux regions of the conventional DTC method and proposed to rotate the flux regions in order to reduce torque ripple. Speed reduction is determined with flux based MRAS and both methods are compared with respect to current, voltage, flux and torque. The proposed method provides significant reduction in a phase current and voltage in the simulation and experimental results. Torque ripple is reduced by about 1/3 Nm with the new method. In addition, the reference flux values are obtained and the flux ripple is reduced by 0.8 Wb compared to the conventional DTC. We present the screen of the spectrum analyzer which is connected to the motor a phase. Without the new method, the current harmonics are around 7.3 % THD and 1 kHz. After applying the new method, THD is decreased to 4.8 % and harmonics around 1 kHz are disappeared. The results suggest that the flux and torque ripple are reduced by rotating the flux regions and adjusting the switching table. Speed, reduced using MRAS, is close enough to the reference speed.

ACKNOWLEDGMENT

The research has been supported by the Research Project Department of Akdeniz University, Antalya, Turkey.

REFERENCES

- [1] X.Li, R. Duke and S. Round., "Development of a three-phase three-level inverter for an electric vehicle", Australasian Universities PowerEngineering Conf., 1999, Darwin, Australia, pp. 247-251.
- [2] Sarioglu M. K., "Fundamentals of Electric Machines I", ITU, Faculty of Electric- Electronic, Offset Press Room,3.Press, 1984.
- [3] Sarioglu M.K., "Gokasan M., Bogosyan S.,Asynchronous Machines and it's Control", Birsen Publishing, ISBN 975-511-343-6, 2003.
- [4] Vasudevan M., Arumugam R., "New Direct Torque Control Scheme of Induction Motor for Electric Vehicles".

